

Analytic two-loop QCD amplitudes for tW production: Leading color and light fermion-loop contributions

Long-Bin Chen,¹ Liang Dong,² Hai Tao Li,² Zhao Li[⊗],^{3,4,5} Jian Wang[⊗],² and Yefan Wang[⊗],^{2,*}

¹*School of Physics and Materials Science, Guangzhou University, Guangzhou 510006, China*

²*School of Physics, Shandong University, Jinan, Shandong 250100, China*

³*Institute of High Energy Physics, Chinese Academy of Sciences, Beijing 100049, China*

⁴*School of Physics Sciences, University of Chinese Academy of Sciences, Beijing 100039, China*

⁵*Center for High Energy Physics, Peking University, Beijing 100871, China*



(Received 7 October 2022; accepted 11 November 2022; published 30 November 2022)

We present the analytical results of the two-loop QCD amplitudes for hadronic tW production, focusing on the leading color and light fermion-loop contributions. The calculation of the two-loop integrals is performed using the method of canonical differential equations. The results have been expressed in terms of multiple polylogarithms and checked by comparing the infrared divergences with the predictions from anomalous dimensions. Combining these with the one-loop squared amplitudes we have computed previously, we obtain the hard function relevant to a next-to-next-to-leading order Monte Carlo calculation. We find that the hard function varies slowly in the region with small top-quark velocity but increases dramatically in the region with large top-quark velocity. After performing phase space integration and convolution with the parton distribution function, the leading color hard function gives a correction of about 5.4% to the leading order cross section, while the light fermion-loop diagrams contribute about -1.4% .

DOI: [10.1103/PhysRevD.106.096029](https://doi.org/10.1103/PhysRevD.106.096029)

I. INTRODUCTION

Single top production can be used to study the electro-weak interaction of the top quark, which is important for the precision test of the Standard Model (SM) and the search for new physics beyond the SM. In particular, the associated production of a top quark with a W boson is sensitive to the Wtb coupling, which has drawn a lot of attention in the community. Recently, precision measurements of the inclusive and differential cross sections of this process have been performed by both ATLAS and CMS collaborations at the Large Hadron Collider (LHC) with $\sqrt{s} = 13$ TeV [1–4]. More precise experimental results will be available in the near future after the launch of the LHC Run 3.

Besides the precision measurements, high precision theoretical predictions are indispensable in extracting useful information from experimental data. At hadron colliders, the QCD corrections are often significant in making reliable predictions, such as reducing the scale uncertainties and

modeling the real process more properly. For tW production, the next-to-leading order (NLO) correction was obtained more than 25 years ago [5], and it was also investigated later in [6–9]. Much effort has been devoted to the studies on the effects beyond NLO QCD corrections, e.g., the expansion to next-to-next-to-next-to-leading order in the threshold limit [10–13] and the all-order threshold resummation [14], which increase the NLO cross section further by a sizable amount on the order of 10%. To provide kinematic distributions with higher-order QCD effects, the prediction with parton showers interfaced with the NLO cross section was explored [15–17].

Unfortunately, the next-to-next-to-leading order (NNLO) QCD prediction of tW production has not been obtained yet. A full NNLO correction consists of the double-real, real-virtual, and double-virtual contributions. In the double-real and real-virtual corrections, it is necessary to define a scheme to clearly distinguish the process of tW production from that of top-quark pair production. This issue has been discussed at NLO [18] and deserves a detailed investigation at NNLO. However, this topic is beyond the scope of this paper, which aims at only the double-virtual contribution. At the cross section level, the double-virtual correction includes the one-loop squared amplitude and the interference between two-loop and tree-level amplitudes. The former has been computed analytically in our previous work [19]. In this paper we present the dominant contribution to the

*wangyefan@sdu.edu.cn

Published by the American Physical Society under the terms of the [Creative Commons Attribution 4.0 International license](https://creativecommons.org/licenses/by/4.0/). Further distribution of this work must maintain attribution to the author(s) and the published article's title, journal citation, and DOI. Funded by SCOAP³.

double-virtual correction, i.e., the leading color and the light fermion-loop results.

This paper is organized as follows. In Sec. II we describe the basic setup and the details in the calculation of two-loop bare amplitudes. We discuss the procedure used to deal with the UV and IR divergences in the bare amplitude in Sec. III. The finite part of the squared amplitude is considered as the hard function, which could be used in a NNLO Monte Carlo calculation. The numerical results for the leading color and light fermion-loop contributions to the NNLO hard function are presented in Sec. IV. Finally, we conclude in Sec. V.

II. TWO-LOOP CALCULATION

A. Kinematics and notations

The tW associated production $g(k_1) + b(k_2) \rightarrow W(k_3) + t(k_4)$ possesses two different massive external particles with $k_3^2 = m_W^2$ and $k_4^2 = (k_1 + k_2 - k_3)^2 = m_t^2$. The initial-state particles are massless, i.e., $k_1^2 = k_2^2 = 0$. The Mandelstam variables are defined by

$$s = (k_1 + k_2)^2, \quad t = (k_1 - k_3)^2, \quad u = (k_2 - k_3)^2, \quad (1)$$

which have the relation $s + t + u = m_W^2 + m_t^2$.

The tree-level scattering amplitude is given by

$$\mathcal{M}^{(0)} = \frac{eg_s t_{4,2}^a}{\sqrt{2} \sin \theta_W} \left(\frac{\bar{u}(k_4) \not{\epsilon}_3^* P_L (\not{k}_3 + \not{k}_4) \not{\epsilon}_1 u(k_2)}{s} + \frac{\bar{u}(k_4) \not{\epsilon}_1 (\not{k}_2 - \not{k}_3 + m_t) \not{\epsilon}_3^* P_L u(k_2)}{u - m_t^2} \right), \quad (2)$$

where $t_{4,2}^a$ is the $SU(3)$ generator with color indices in the subscript corresponding to the top and bottom quarks. The polarization vectors for the gluon and the W boson are denoted by ϵ_1^μ and $\epsilon_3^{*\mu}$, respectively. Here, $P_L = (1 - \gamma_5)/2$ is the left-handed projection operator.

We do not consider the decay of the top quark and the W boson yet, and thus we sum over the polarization states of the gauge bosons in the amplitude squared. Specifically, we apply the equation

$$\sum_i \epsilon_i^{*\mu}(k_3) \epsilon_i^\nu(k_3) = -g^{\mu\nu} + \frac{k_3^\mu k_3^\nu}{m_W^2} \quad (3)$$

for the W boson, and

$$\sum_i \epsilon_i^\mu(k_1) \epsilon_i^{*\nu}(k_1) = -g^{\mu\nu} + \frac{n^\mu k_1^\nu + n^\nu k_1^\mu}{n \cdot k_1} \quad (4)$$

for the gluon, where n^μ denotes a lightlike vector. We have chosen a physical gauge for the gluon, so we do not need to consider the contribution from ghost particles in the external states. In practice, we can simply neglect the

second term in the above equation because of the Ward identity.

In this work, we calculate the interference between the two-loop, denoted by $\mathcal{M}^{(2)}$, and tree-level amplitudes, which can be decomposed according to the color and flavor structures,

$$\begin{aligned} \mathcal{A}^{(2)} = 2\text{Re} \sum_{\text{spin,color}} \mathcal{M}^{(0)*} \mathcal{M}^{(2)} &= N_c^4 A + N_c^2 B + C + \frac{1}{N_c^2} D \\ &+ n_l \left(N_c^3 E_l + N_c F_l + \frac{1}{N_c} G_l \right) \\ &+ n_h \left(N_c^3 E_h + N_c F_h + \frac{1}{N_c} G_h \right), \end{aligned} \quad (5)$$

where n_l and n_h are the total numbers of light and heavy quark flavors, respectively, and A, B, C, D, E, F, G are the corresponding coefficients. Notice that we do not perform a color average for the initial states in the squared amplitude. Therefore, the leading contribution is proportional to N_c^4 (or N_c^3 for fermion-loop contributions). The following terms are suppressed by N_c^2 in sequence. The fact that color-summed squared amplitudes can be expanded in a series of $1/N_c^2$, rather than $1/N_c$, has been discussed in detail at the one-loop level in [20]. In our case, this expansion pattern can be understood. The Wtb vertex does not affect the color flow and thus can be omitted in the analysis of color structure.¹ As a result, the structure of a color-summed squared amplitude is represented by the vacuum graph; see Fig. 1 for a few examples. When analyzing the color factors of squared amplitudes, the four-gluon vertex in a graph is replaced by two three-gluon vertices, and any three-gluon vertex is substituted by a difference of two fermion loops due to the identity

$$if^{abc} = 2(\text{Tr}[t^a t^b t^c] - \text{Tr}[t^a t^c t^b]). \quad (6)$$

Now, all the color structure in the graph is a combination of traces of multiple color generators t^a . Applying the $SU(N_c)$ Fierz identity

$$t_{ij}^a t_{kl}^a = \frac{1}{2} \delta_{il} \delta_{kj} - \frac{1}{2N_c} \delta_{ij} \delta_{kl} \quad (7)$$

to contract the color indices carried by each gluon propagator, the resulting color structure consists of only δ_{ii} , each of which contributes a factor of N_c .² The leading color (or color planar) contribution is obtained by taking only the first term in Eq. (7). The second term not only contains a

¹This means that the quark flavor does not change along the fermion line.

²This can be illustrated by decomposing every vacuum graph to several fermion loops after replacing each gluon with either a quark-antiquark pair or simply dropping it.

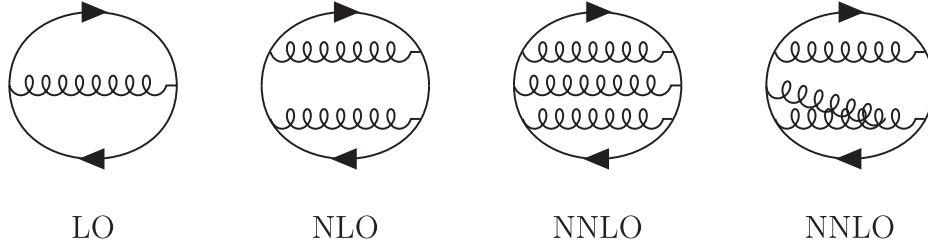


FIG. 1. Typical color structure of the squared amplitudes at LO, NLO, and NNLO.

factor of $1/N_c$ but also reduces the number of δ_{ii} (or fermion loops in a graph) due to the color flow topology. When there is a three-gluon vertex, one of the terms in Eq. (6) gives rise to the leading color contribution, while the other generates a graph with two fewer fermion loops. In any case, the expansion is in a series of $1/N_c^2$. In QCD, this factor is of the same magnitude as the strong coupling and serves as a good perturbative expansion parameter. In addition, the result at each order in this expansion is gauge invariant and could be calculated independently. Due to the simple topology of the Feynman diagrams contributing to the leading color,³ the calculation of this part is notably easier than the full two-loop corrections. Therefore, we constrain ourselves to present the result at leading color in this paper, i.e., the coefficient A in Eq. (5). As the number of light quarks in the loop is larger than N_c and the needed master integrals are almost the same, we also provide the result proportional to n_l . In summary, we have calculated the following gauge invariant contribution to two-loop squared amplitudes:

$$\mathcal{A}_{\text{L.C.}+n_l}^{(2)} \equiv N_c^4 A + n_l \left(N_c^3 E_l + N_c F_l + \frac{1}{N_c} G_l \right). \quad (8)$$

B. Bare two-loop amplitudes

All the two-loop Feynman diagrams for the process $gb \rightarrow Wt$ are generated by using FeynArts [21]. There are 199 two-loop Feynman diagrams in total, of which 73 diagrams contribute to the leading color and 20 diagrams have a light fermion loop. Some typical two-loop Feynman diagrams are displayed in Fig. 2. We compute the interference between two-loop and tree-level amplitudes directly, and thus there are no Lorentz indices remaining in the spin-summed result. The traces of Dirac matrices are performed using the package FeynCalc [22]. We use the conventional dimensional regularization scheme to deal with both the UV and IR divergences; i.e., the space-time dimension is extended to $d = 4 - 2\epsilon$. The anticommuting γ_5 scheme is adopted following Ref. [23]. The traces containing two γ_5 matrices are trivial due to $\gamma_5^2 = 1$ after

³Here the terminology ‘‘topology’’ includes the information on the masses of internal propagators.

moving the two γ_5 matrices adjacent to each other. The traces with a single γ_5 matrix are vanishing in our problem because there are only three independent momenta involved. More detailed discussions can be found in Ref. [19].

As a consequence, we obtain the squared amplitude as a linear combination of a large number of scalar Feynman integrals with rational coefficients depending on the kinematic invariants s, t, u and the space-time dimension d . We find that all the squared amplitudes contributing to the leading color can be expressed in terms of the integrals appearing in the Feynman diagrams shown in Fig. 2. Explicitly, they are given by

$$I_{n_1, n_2, \dots, n_9}^{\text{L.C.}} = \int \frac{d^d q_1}{i\pi^{d/2}} \frac{d^d q_2}{i\pi^{d/2}} e^{2\gamma_E \epsilon} \frac{D_8^{-n_8} D_9^{-n_9}}{D_1^{n_1} D_2^{n_2} \dots D_7^{n_7}}, \quad (9)$$

where q_1 and q_2 are loop momenta and D_i with $i = 1, \dots, 7$ denote the denominators of the propagators in each Feynman diagram in Fig. 2.⁴ The other two denominators D_8 and D_9 are added in order to provide a complete basis for all possible Lorentz invariant scalar products formed by two loop momenta and three external momenta.

All of these integrals are then reduced to a small set of basis integrals, called master integrals, using the relations generated by integration-by-parts (IBP) identities. We have made use of the package FIRE [24] in this step. After considering the symmetry between different topologies, all the two-loop master integrals can be categorized into only two integral families, as displayed in Fig. 3.⁵ The denominators for P1 are given by

$$\begin{aligned} D_1 &= q_1^2, & D_2 &= q_2^2, & D_3 &= (q_1 - k_1)^2, \\ D_4 &= (q_1 + k_2)^2, & D_5 &= (q_1 + q_2 - k_1)^2, \\ D_6 &= (q_2 - k_1 - k_2)^2, & D_7 &= (q_2 - k_3)^2 - m_t^2, \\ D_8 &= (q_1 + k_1 + k_2 - k_3)^2 - m_t^2, & D_9 &= (q_2 - k_1)^2, \end{aligned} \quad (10)$$

⁴Here we abuse the notation of D_i . In principle, each Feynman diagram has a set of seven denominators. They are not the same in other diagrams.

⁵Here we do not include the master integrals that can be factorized as two one-loop integrals, which are easy to calculate [19].

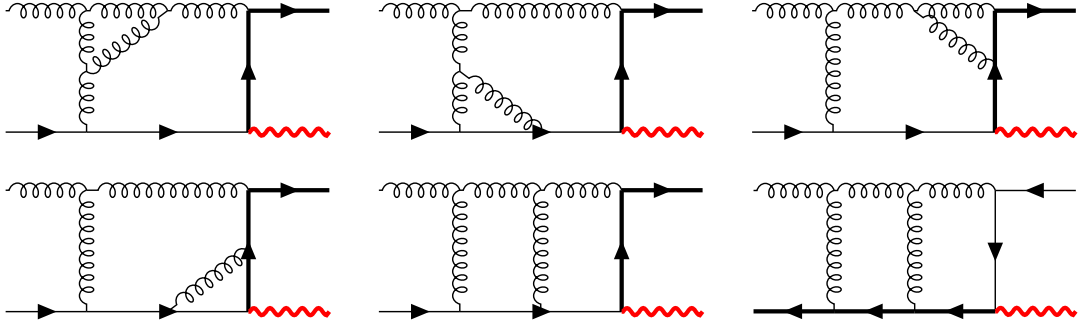


FIG. 2. Typical two-loop leading color Feynman diagrams for tW production. The thick black and red lines stand for the top quark and the W boson, respectively.

and the denominators for P2 are

$$\begin{aligned}
 D_1 &= q_1^2, & D_2 &= q_2^2, & D_3 &= (q_1 - k_2)^2, \\
 D_4 &= (q_1 - k_3)^2 - m_t^2, & D_5 &= (q_1 + q_2 - k_2)^2, & D_6 &= (q_2 + k_1)^2, \\
 D_7 &= (q_2 - k_2 + k_3)^2 - m_t^2, & D_8 &= (q_1 - k_1 - k_2)^2, & D_9 &= (q_2 + k_1 - k_2)^2.
 \end{aligned} \tag{11}$$

There are 31 and 38 master integrals in the P1 and P2 integral families, respectively. We have calculated them using the method of differential equations [25,26]. Taking the derivative of one master integral with respect to a kinematic variable, e.g., s , the result can be written as a linear combination of the master integrals since all integrals in a family can be reduced back to the basis. These differential equations incorporate almost all the information about the integrals. One can choose a proper kinematic point where the integrals are relatively easier to compute either analytically or numerically, and derive the values at other kinematic points by solving the differential equations. The latter is simplified if a canonical basis can be found, i.e., the differential equations can be transformed to a form in which the dimensional regulator ϵ is decoupled from the kinematic variables [27]. This is called the ϵ form or $d \ln$ form. A formal solution to this differential equation is given in terms of Chen iterated integrals [28]. If the involved symbol letters, i.e., the arguments of the $d \ln$ form, are polynomials of the integration variables, the solution can be expressed as multiple polylogarithms [29], which are defined as $G(x) \equiv 1$ and

$$G_{a_1, a_2, \dots, a_n}(x) \equiv \int_0^x \frac{dt}{t - a_1} G_{a_2, \dots, a_n}(t), \tag{12}$$

$$G_{\bar{0}_n}(x) \equiv \frac{1}{n!} \ln^n x. \tag{13}$$

The number of elements in the set (a_1, a_2, \dots, a_n) is referred to as the transcendental weight of the multiple polylogarithms. For the two-loop amplitudes, we need multiple polylogarithms up to transcendental weight four, and we use PolyLogTools [30], which relies on the GiNaC package [31,32], to perform efficient numerical evaluation of these functions. The analytical results of the P1 integral family have been obtained by two of the authors [33], while the master integrals in the P2 family have been calculated in [34], and also independently checked by [35].

Then, we consider the squared amplitude containing a light fermion loop. Using the same method as discussed above, we reduce all the scalar integrals to a set of master integrals. In addition to those already appearing in the P1 and P2 integral families, another integral family with two massive propagators, as shown in Fig. 4, should be taken into account. Explicitly, this is defined as

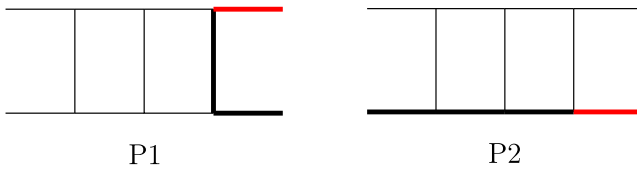


FIG. 3. Unfactorized two-loop master integral topologies relevant to the leading color contribution. The thick black and red lines stand for the top quark and the W boson, respectively. The other lines denote massless particles.

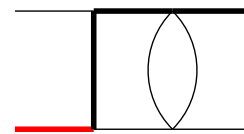


FIG. 4. Integral topology appearing in the light fermion-loop contribution. The thick black and red lines stand for the top quark and the W boson, respectively. The other lines denote massless particles.

$$I_{n_1, n_2, n_3, n_4, n_5, n_6, n_7, n_8, n_9} = \int \frac{d^d q_1}{i\pi^{d/2}} \frac{d^d q_2}{i\pi^{d/2}} e^{2\gamma_E \epsilon} \frac{[q_2^2]^{-n_6} [(q_2 - k_1 + k_3)^2]^{-n_7} [(q_2 - k_2 + k_3)^2]^{-n_8} [(q_1 - k_3 + k_2)^2]^{-n_9}}{[q_1^2 - m_t^2]^{n_1} [(q_1 - k_1)^2 - m_t^2]^{n_2} [(q_1 - k_3)^2]^{n_3} [(q_1 + q_2 - k_1)^2]^{n_4} [(q_2 - k_4)^2]^{n_5}}. \quad (14)$$

Since the result of this integral family is still unknown, we present more details here. We choose the following canonical basis:

$$\begin{aligned} g_1 &= \epsilon^2 m_t^2 M_1, \\ g_2 &= \epsilon^2 u M_2, \\ g_3 &= \epsilon^2 ((u - m_t^2) M_3 - 2m_t^2 M_2), \\ g_4 &= \epsilon^3 (t - m_t^2) M_4, \\ g_5 &= \epsilon^3 (u - m_W^2) M_5, \\ g_6 &= \epsilon^3 (1 - 2\epsilon) (t - m_W^2) M_6, \\ g_7 &= \epsilon^3 (t - m_t^2) (u - m_t^2) M_7, \end{aligned} \quad (15)$$

where

$$\begin{aligned} M_1 &= I_{0,2,0,2,1,0,0,0,0}, & M_2 &= I_{2,0,0,2,1,0,0,0,0}, \\ M_3 &= I_{1,0,0,2,2,0,0,0,0}, & M_4 &= I_{0,1,1,1,2,0,0,0,0}, \\ M_5 &= I_{1,0,1,1,2,0,0,0,0}, & M_6 &= I_{1,1,1,1,1,0,0,0,0}, \\ M_7 &= I_{1,1,1,1,2,0,0,0,0}. \end{aligned} \quad (16)$$

The corresponding topology diagrams are displayed in Fig. 5.

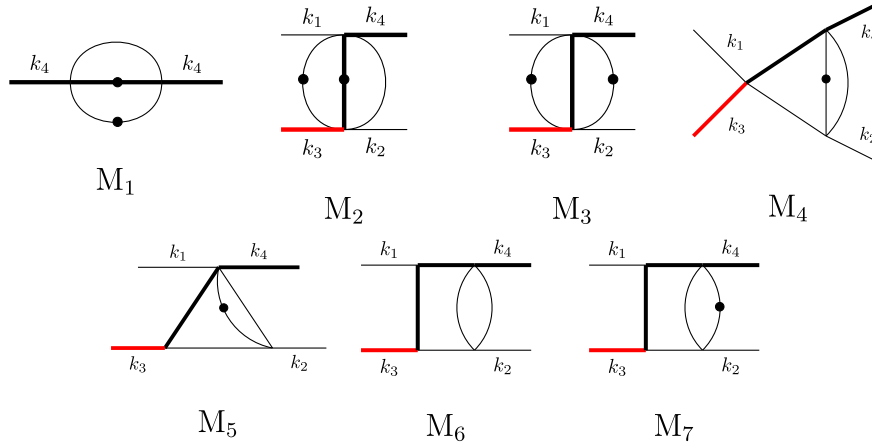


FIG. 5. Topology diagrams for the master integrals defined in Eq. (14). The thick (thin) black lines stand for the massive (massless) quark, and the thick red lines represent the W boson. The black dot indicates one additional power of the corresponding propagator.

The differential equations for the canonical basis $\mathbf{g} = (g_1, \dots, g_7)$ can be formulated as

$$d\mathbf{g}(x, y, z; \epsilon) = \epsilon(d\tilde{A})\mathbf{g}(x, y, z; \epsilon) \quad (17)$$

with

$$d\tilde{A} = \sum_{i=1}^{10} R_i d \ln(l_i). \quad (18)$$

The letters are given by

$$\begin{aligned} l_1 &= x, & l_2 &= x - 1, \\ l_3 &= y, & l_4 &= y - 1, \\ l_5 &= z, & l_6 &= z - 1, \\ l_7 &= x - z, & l_8 &= xy - z, \\ l_9 &= 1 + z - x - y, & l_{10} &= y - z, \end{aligned} \quad (19)$$

with

$$x = \frac{t}{m_t^2}, \quad y = \frac{u}{m_t^2}, \quad z = \frac{m_W^2}{m_t^2}. \quad (20)$$

The rational matrices R_i are

$$\begin{aligned}
R_1 &= \begin{pmatrix} 0 & 0 & 0 & 0 & 0 & 0 & 0 \\ 0 & 0 & 0 & 0 & 0 & 0 & 0 \\ 0 & 0 & 0 & 0 & 0 & 0 & 0 \\ -1 & 0 & 0 & 2 & 0 & 0 & 0 \\ 0 & 0 & 0 & 0 & 0 & 0 & 0 \\ -1 & 0 & 0 & 2 & 0 & 0 & 0 \\ 0 & 0 & 0 & 0 & 0 & 0 & 0 \end{pmatrix}, & R_2 &= \begin{pmatrix} 0 & 0 & 0 & 0 & 0 & 0 & 0 \\ 0 & 0 & 0 & 0 & 0 & 0 & 0 \\ 0 & 0 & 0 & 0 & 0 & 0 & 0 \\ 0 & 0 & 0 & -4 & 0 & 0 & 0 \\ 0 & 0 & 0 & 0 & 0 & 0 & 0 \\ 0 & 0 & 0 & 0 & 0 & 0 & 0 \\ 0 & 0 & 0 & 0 & 0 & 0 & -4 \end{pmatrix}, \\
R_3 &= \begin{pmatrix} 0 & 0 & 0 & 0 & 0 & 0 & 0 \\ 0 & 1 & 0 & 0 & 0 & 0 & 0 \\ 0 & 4 & 0 & 0 & 0 & 0 & 0 \\ 0 & 0 & 0 & 0 & 0 & 0 & 0 \\ 0 & -1 & 0 & 0 & 0 & 0 & 0 \\ 0 & 0 & 0 & 0 & 0 & 0 & 0 \\ 0 & 0 & 0 & 0 & 0 & 0 & 0 \end{pmatrix}, & R_4 &= \begin{pmatrix} 0 & 0 & 0 & 0 & 0 & 0 & 0 \\ 0 & -2 & -1 & 0 & 0 & 0 & 0 \\ 0 & -4 & -2 & 0 & 0 & 0 & 0 \\ 0 & 0 & 0 & 0 & 0 & 0 & 0 \\ 0 & 1 & \frac{1}{2} & 0 & 0 & 0 & 0 \\ -2 & 1 & -\frac{1}{2} & 0 & 0 & 0 & 0 \\ 0 & 0 & 0 & 0 & 0 & 0 & -4 \end{pmatrix}, \\
R_5 &= \begin{pmatrix} 0 & 0 & 0 & 0 & 0 & 0 & 0 \\ 0 & 0 & 0 & 0 & 0 & 0 & 0 \\ 0 & 0 & 0 & 0 & 0 & 0 & 0 \\ 0 & 0 & 0 & 0 & 0 & 0 & 0 \\ 0 & 1 & 0 & 0 & 2 & 0 & 0 \\ 0 & 1 & 0 & 0 & 2 & 0 & 0 \\ 0 & 0 & 0 & 0 & 0 & 0 & 0 \end{pmatrix}, & R_6 &= \begin{pmatrix} 0 & 0 & 0 & 0 & 0 & 0 & 0 \\ 0 & 0 & 0 & 0 & 0 & 0 & 0 \\ 0 & 0 & 0 & 0 & 0 & 0 & 0 \\ 0 & 0 & 0 & 0 & 0 & 0 & 0 \\ 0 & -1 & -\frac{1}{2} & 0 & -3 & 0 & 0 \\ 0 & 0 & 0 & 0 & 0 & 0 & 0 \\ 0 & -1 & -\frac{1}{2} & 0 & -3 & 0 & 0 \end{pmatrix}, \\
R_7 &= \begin{pmatrix} 0 & 0 & 0 & 0 & 0 & 0 & 0 \\ 0 & 0 & 0 & 0 & 0 & 0 & 0 \\ 0 & 0 & 0 & 0 & 0 & 0 & 0 \\ 0 & 0 & 0 & 0 & 0 & 0 & 0 \\ 0 & 0 & 0 & 0 & 0 & 0 & 0 \\ 0 & 0 & 0 & 0 & 0 & 1 & 0 \\ 0 & 1 & \frac{1}{2} & 3 & 3 & 0 & 1 \end{pmatrix}, & R_8 &= \begin{pmatrix} 0 & 0 & 0 & 0 & 0 & 0 & 0 \\ 0 & 0 & 0 & 0 & 0 & 0 & 0 \\ 0 & 0 & 0 & 0 & 0 & 0 & 0 \\ 0 & 0 & 0 & 0 & 0 & 0 & 0 \\ 0 & 0 & 0 & 0 & 0 & 0 & 0 \\ 1 & -\frac{1}{2} & \frac{1}{4} & -\frac{1}{2} & -\frac{1}{2} & -\frac{1}{2} & \frac{1}{2} \\ 3 & -\frac{3}{2} & \frac{3}{4} & -\frac{3}{2} & -\frac{3}{2} & -\frac{3}{2} & \frac{3}{2} \end{pmatrix}, \\
R_9 &= \begin{pmatrix} 0 & 0 & 0 & 0 & 0 & 0 & 0 \\ 0 & 0 & 0 & 0 & 0 & 0 & 0 \\ 0 & 0 & 0 & 0 & 0 & 0 & 0 \\ 0 & 0 & 0 & 0 & 0 & 0 & 0 \\ 0 & 0 & 0 & 0 & 0 & 0 & 0 \\ 1 & -\frac{1}{2} & \frac{1}{4} & \frac{1}{2} & \frac{1}{2} & -\frac{1}{2} & -\frac{1}{2} \\ -3 & \frac{3}{2} & -\frac{3}{4} & -\frac{3}{2} & -\frac{3}{2} & \frac{3}{2} & \frac{3}{2} \end{pmatrix}, & R_{10} &= \begin{pmatrix} 0 & 0 & 0 & 0 & 0 & 0 & 0 \\ 0 & 0 & 0 & 0 & 0 & 0 & 0 \\ 0 & 0 & 0 & 0 & 0 & 0 & 0 \\ 0 & 0 & 0 & 0 & 0 & 0 & 0 \\ 0 & 0 & 0 & 0 & -1 & 0 & 0 \\ 0 & 0 & 0 & 0 & 0 & 0 & 0 \\ 0 & 0 & 0 & 0 & 3 & 0 & 0 \end{pmatrix}. \tag{21}
\end{aligned}$$

The basis integral g_1 is simple and can be calculated directly [36],

$$g_1 = -\frac{1}{4} - \epsilon^2 \frac{5\pi^2}{24} - \epsilon^3 \frac{11\zeta(3)}{6} - \epsilon^4 \frac{101\pi^4}{480} + \mathcal{O}(\epsilon^5). \tag{22}$$

The boundary condition for g_3 is chosen at $u = 0$,

$$g_3|_{u=0} = 1 + \epsilon^2 \frac{\pi^2}{2} - \epsilon^3 \frac{8\zeta(3)}{3} + \epsilon^4 \frac{7\pi^4}{40} + \mathcal{O}(\epsilon^5). \quad (23)$$

The boundary conditions of other basis integrals g_i can be found using the regularity conditions. We know that the integrals g_i do not contain any branch cut starting at the points corresponding to $m_W^2 = 0$, $s = m_t^2$, $u = 0$, or $t = 0$. Therefore, the derivatives of the integrals do not have poles at these points, which can generate relations among the integrals that appear as coefficients of the poles.

With these boundary conditions, it is easy to obtain the analytical results for the canonical basis. The integration path from the boundary point to the physical point does not cross over any branch cut in this case, and thus there is no need to perform analytic continuation. Consequently, the integrals in the above family are real in the relevant physical region satisfying

$$\begin{aligned} s &> (m_t + m_W)^2, \\ \frac{m_t^2 + m_W^2 - s - r}{2} &< t < \frac{m_t^2 + m_W^2 - s + r}{2}, \\ 0 &< m_W^2 < m_t^2 \end{aligned} \quad (24)$$

with $r = \sqrt{s - (m_t - m_W)^2} \sqrt{s - (m_t + m_W)^2}$.

III. UV AND IR DIVERGENCES

A. Renormalization

After the calculation of two-loop Feynman diagrams, the bare amplitude, denoted by $\mathcal{M}_{\text{bare}}$, contains UV and IR divergences. To cancel the UV divergence, we generate the Feynman diagrams with the counterterms, which arise from the renormalization of the couplings, masses, and field strength. Then, the renormalized QCD amplitude is obtained by

$$\mathcal{M}_{\text{ren}} = Z_g^{1/2} Z_b^{1/2} Z_t^{1/2} (\mathcal{M}_{\text{bare}}|_{\alpha_s^{\text{bare}} \rightarrow Z_{\alpha_s} \alpha_s; m_t^{\text{bare}} \rightarrow Z_m m_t}), \quad (25)$$

where $Z_{g,b,t}$ are the wave-function renormalization factors for the external colored particles. The strong coupling α_s and top-quark mass are renormalized by the factors Z_{α_s} and Z_m , respectively. In our notation, the amplitude and renormalization factors are expanded as a series of $\alpha_s/4\pi$, e.g.,

$$Z_x = 1 + \frac{\alpha_s}{4\pi} \delta Z_x^{(1)} + \left(\frac{\alpha_s}{4\pi}\right)^2 \delta Z_x^{(2)}.$$

The renormalized amplitude is

$$\begin{aligned} \mathcal{M}_{\text{ren}} &= \mathcal{M}_{\text{bare}}^{(0)} + \frac{\alpha_s}{4\pi} (\mathcal{M}_{\text{bare}}^{(1)} + \mathcal{M}_{\text{C.T.}}^{(1)}) \\ &\quad + \left(\frac{\alpha_s}{4\pi}\right)^2 (\mathcal{M}_{\text{bare}}^{(2)} + \mathcal{M}_{\text{C.T.}}^{(2)}) \\ &= \mathcal{M}_{\text{ren}}^{(0)} + \frac{\alpha_s}{4\pi} \mathcal{M}_{\text{ren}}^{(1)} + \left(\frac{\alpha_s}{4\pi}\right)^2 \mathcal{M}_{\text{ren}}^{(2)} \end{aligned} \quad (26)$$

with the counterterm contribution

$$\begin{aligned} \mathcal{M}_{\text{C.T.}}^{(1)} &= \delta Z_1 \mathcal{M}_{\text{ren}}^{(0)} + \delta Z_m^{(1)} \mathcal{M}_{\text{C.T.}}^{(0),m_t}, \\ \mathcal{M}_{\text{C.T.}}^{(2)} &= \delta Z_2 \mathcal{M}_{\text{ren}}^{(0)} + \delta Z_3 \mathcal{M}_{\text{bare}}^{(1)} + \delta Z_4 \mathcal{M}_{\text{C.T.}}^{(0),m_t} \\ &\quad + (\delta Z_m^{(1)})^2 \mathcal{M}_{\text{C.T.}}^{(0),m_t} + \delta Z_m^{(1)} \mathcal{M}_{\text{C.T.}}^{(1),m_t}. \end{aligned} \quad (27)$$

Here, $\mathcal{M}_{\text{C.T.}}^{(0),m_t}$ ($\mathcal{M}_{\text{C.T.}}^{(1),m_t}$) denotes the amplitude with an insertion of a mass counterterm vertex in the tree-level (one-loop) Feynman diagrams, while $\mathcal{M}_{\text{C.T.}}^{(0),m_t}$ contains two such mass counterterm vertices in the tree-level Feynman diagrams. The definitions of δZ_i in Eq. (27) are given by

$$\begin{aligned} \delta Z_1 &= \frac{1}{2} [\delta Z_g^{(1)} + \delta Z_b^{(1)} + \delta Z_t^{(1)} + \delta Z_{\alpha_s}^{(1)}], \\ \delta Z_2 &= \frac{1}{2} [\delta Z_g^{(2)} + \delta Z_b^{(2)} + \delta Z_t^{(2)} + \delta Z_{\alpha_s}^{(2)}] + \frac{1}{4} [\delta Z_g^{(1)} \delta Z_b^{(1)} \\ &\quad + \delta Z_g^{(1)} \delta Z_t^{(1)} + \delta Z_b^{(1)} \delta Z_t^{(1)} + \delta Z_g^{(1)} \delta Z_{\alpha_s}^{(1)} \\ &\quad + \delta Z_b^{(1)} \delta Z_{\alpha_s}^{(1)} + \delta Z_t^{(1)} \delta Z_{\alpha_s}^{(1)}] \\ &\quad - \frac{1}{8} [(\delta Z_g^{(1)})^2 + (\delta Z_b^{(1)})^2 + (\delta Z_t^{(1)})^2 + (\delta Z_{\alpha_s}^{(1)})^2], \\ \delta Z_3 &= \delta Z_1 + \delta Z_{\alpha_s}^{(1)}, \\ \delta Z_4 &= \delta Z_1 \delta Z_m^{(1)} + \delta Z_m^{(2)}. \end{aligned} \quad (28)$$

Notice that those quantities in Eq. (26) should be calculated in d -dimensional space-time and kept up to $\mathcal{O}(\epsilon^0)$.

We have adopted the on-shell scheme for the renormalization of the wave functions and the top-quark mass. The strong coupling α_s is renormalized in the $\overline{\text{MS}}$ scheme. Up to two loops, the relevant renormalization constants are given by [37–40]

$$\begin{aligned}
Z_g &= 1 + \left(\frac{\alpha_s}{4\pi}\right) T_F n_h D_\epsilon \left(-\frac{4}{3\epsilon}\right) + \left(\frac{\alpha_s}{4\pi}\right)^2 T_F n_h D_\epsilon^2 \left[C_F \left(-\frac{2}{\epsilon} - 15\right) + C_A \left(\frac{35}{9\epsilon^2} - \frac{5}{2\epsilon} + \frac{13}{12}\right) - \frac{16}{9\epsilon^2} T_F n_l - \frac{\pi^2}{9} \beta_0 \right. \\
&\quad \left. + \frac{4}{3} \beta_0 \ln\left(\frac{\mu^2}{m_t^2}\right) \left(-\frac{1}{\epsilon} + \frac{1}{2} \ln\left(\frac{\mu^2}{m_t^2}\right)\right) \right], \\
Z_b &= 1 + \left(\frac{\alpha_s}{4\pi}\right)^2 C_F T_F n_h D_\epsilon^2 \left(\frac{1}{\epsilon} - \frac{5}{6}\right), \\
Z_t &= 1 + \left(\frac{\alpha_s}{4\pi}\right) C_F D_\epsilon \left(-\frac{3}{\epsilon} - 4 - 8\epsilon - 16\epsilon^2\right) + \left(\frac{\alpha_s}{4\pi}\right)^2 C_F D_\epsilon^2 \left[T_F n_h \left(\frac{1}{\epsilon} + \frac{947}{18} - 5\pi^2\right) \right. \\
&\quad \left. + T_F n_l \left(-\frac{2}{\epsilon^2} + \frac{11}{3\epsilon} + \frac{113}{6} + \frac{5\pi^2}{3}\right) + C_F \left(\frac{9}{2\epsilon^2} + \frac{51}{4\epsilon} + \frac{433}{8} - 13\pi^2 + 16\pi^2 \ln 2 - 24\zeta_3\right) \right. \\
&\quad \left. + C_A \left(\frac{11}{2\epsilon^2} - \frac{127}{12\epsilon} - \frac{1705}{24} + \frac{49\pi^2}{12} - 8\pi^2 \ln 2 + 12\zeta_3\right) \right. \\
&\quad \left. + \beta_0 \ln\left(\frac{\mu^2}{m_t^2}\right) \left(-\frac{3}{\epsilon} - 4 + \frac{3}{2} \ln\left(\frac{\mu^2}{m_t^2}\right)\right) \right], \\
Z_m &= 1 + \left(\frac{\alpha_s}{4\pi}\right) C_F D_\epsilon \left(-\frac{3}{\epsilon} - 4 - 8\epsilon - 16\epsilon^2\right) + \left(\frac{\alpha_s}{4\pi}\right)^2 C_F D_\epsilon^2 \left[\beta_0 \left(\frac{3}{2\epsilon^2} - \frac{5}{4\epsilon} - \frac{143}{8} + \frac{7\pi^2}{4}\right) + 4T_F n_l (-3 + \pi^2) \right. \\
&\quad \left. + C_F \left(\frac{9}{2\epsilon^2} + \frac{45}{4\epsilon} + \frac{199}{8} - 5\pi^2 + 8\pi^2 \ln 2 - 12\zeta_3\right) + C_A \left(-\frac{7}{2\epsilon} + \frac{77}{4} - 6\pi^2 - 4\pi^2 \ln 2 + 6\zeta_3\right) \right. \\
&\quad \left. + \beta_0 \ln\left(\frac{\mu^2}{m_t^2}\right) \left(-\frac{3}{\epsilon} - 4 + \frac{3}{2} \ln\left(\frac{\mu^2}{m_t^2}\right)\right) \right], \\
Z_{\alpha_s} &= 1 - \frac{\alpha_s \beta_0}{4\pi \epsilon} + \left(\frac{\alpha_s}{4\pi}\right)^2 \left(\frac{\beta_0^2}{\epsilon^2} - \frac{\beta_1}{2\epsilon}\right), \tag{29}
\end{aligned}$$

where

$$\begin{aligned}
D_\epsilon &\equiv e^{\gamma_E \epsilon} \Gamma(1 + \epsilon) \left(\frac{\mu^2}{m_t^2}\right)^\epsilon, \\
\beta_0 &= \frac{11}{3} C_A - \frac{4}{3} T_F (n_l + n_h), \\
\beta_1 &= \frac{34}{3} C_A^2 - \frac{20}{3} C_A T_F (n_l + n_h) - 4 C_F T_F (n_l + n_h), \tag{30}
\end{aligned}$$

with $n_l = 5$ and $n_h = 1$ for the process $gb \rightarrow Wt$.

B. IR divergences

The renormalized amplitudes in Eq. (26) still contain IR divergences, which have a general structure that depends only on the properties of external particles. These divergences can be factorized from the finite part of the amplitudes because of the properties of the amplitudes in the soft and collinear limits [41–47], i.e.,

$$\mathcal{M}_{\text{ren}} = \mathbf{Z} \mathcal{M}_{\text{fin}}, \tag{31}$$

where the factor \mathbf{Z} encodes all the IR divergences of the scattering amplitudes and has been computed to two loops for general processes with massive particles. For single top

production, the IR divergences have been studied at three-loop level [48]; see [49] for more general processes.

The IR divergences of the amplitudes in QCD can be reproduced by the corresponding amplitudes in the soft-collinear effective theory (SCET). As such, the IR divergences are transformed into UV ones since all the loop integrals in the effective theory are scaleless and thus vanish in dimensional regularization. These UV divergences are closely related to the anomalous dimensions of effective operators corresponding to the relevant process. For $gb \rightarrow Wt$, the anomalous dimension Γ_h up to two loops is given by

$$\begin{aligned}
\Gamma_h &= \mathbf{T}_1 \cdot \mathbf{T}_2 \gamma_{\text{cusp}}(\hat{\alpha}_s) \ln \frac{\mu^2}{-s} + \mathbf{T}_1 \cdot \mathbf{T}_4 \gamma_{\text{cusp}}(\hat{\alpha}_s) \ln \frac{m_t \mu}{m_t^2 - u} \\
&\quad + \mathbf{T}_2 \cdot \mathbf{T}_4 \gamma_{\text{cusp}}(\hat{\alpha}_s) \ln \frac{m_t \mu}{m_t^2 - t} + \gamma_g(\hat{\alpha}_s) \\
&\quad + \gamma_q(\hat{\alpha}_s) + \gamma_t(\hat{\alpha}_s) \\
&= \frac{\gamma_{\text{cusp}}(\hat{\alpha}_s)}{2} \left(-C_A \ln \frac{\mu^2}{-s} - C_A \ln \frac{m_t \mu}{m_t^2 - u} \right. \\
&\quad \left. + (C_A - 2C_F) \ln \frac{m_t \mu}{m_t^2 - t} \right) \\
&\quad + \gamma_g(\hat{\alpha}_s) + \gamma_q(\hat{\alpha}_s) + \gamma_t(\hat{\alpha}_s), \tag{32}
\end{aligned}$$

where \mathbf{T}_i is the color charge associated with the external particle i , as defined in [50]. The anomalous dimensions γ_{cusp} , γ_g , γ_b , and γ_t are universal quantities in the sense that they are independent of the hard scattering process. Their two-loop expressions can be found in the appendix of [51]. Here we use the notation $\hat{\alpha}_s$ for the strong coupling with five light quark flavors in its anomalous dimension. The matching to the coupling α_s involving heavy quarks in its renormalization is given by $\alpha_s = \xi \hat{\alpha}_s$ with [45,52]

$$\xi = 1 + \frac{\alpha_s}{3\pi} T_F n_h \frac{D_\epsilon - 1}{\epsilon} + \mathcal{O}(\alpha_s^2). \quad (33)$$

Then, the \mathbf{Z} factor can be obtained by

$$\begin{aligned} \ln \mathbf{Z} &= \frac{\alpha_s}{4\pi} \frac{1}{\xi} \left[\frac{\Gamma'_h(0)}{4\epsilon^2} + \frac{\Gamma_h(0)}{2\epsilon} \right] \\ &+ \left(\frac{\alpha_s}{4\pi} \right)^2 \frac{1}{\xi^2} \left[\frac{-3\hat{\beta}_0 \Gamma'_h(0)}{16\epsilon^3} + \frac{\Gamma'_h(1) - 4\hat{\beta}_0 \Gamma_h(0)}{16\epsilon^2} + \frac{\Gamma_h(1)}{4\epsilon} \right] \\ &+ \mathcal{O}(\alpha_s^3), \end{aligned} \quad (34)$$

where $\hat{\beta}_0$ is the LO β function for the coupling $\hat{\alpha}_s$ in SCET and thus $\hat{\beta}_0 = \beta_0|_{n_h \rightarrow 0}$. We have defined $\Gamma'_h = \partial \Gamma_h / \partial \ln \mu$. With all the ingredients at hand, it is straightforward to compute \mathbf{Z} in the expansion form

$$\mathbf{Z} = 1 + \frac{\alpha_s}{4\pi} \mathbf{Z}^{(1)} + \left(\frac{\alpha_s}{4\pi} \right)^2 \mathbf{Z}^{(2)} + \mathcal{O}(\alpha_s^3). \quad (35)$$

The finite amplitude up to two loops can be written as

$$\mathcal{M}_{\text{fin}} = \mathcal{M}_{\text{fin}}^{(0)} + \frac{\alpha_s}{4\pi} \mathcal{M}_{\text{fin}}^{(1)} + \left(\frac{\alpha_s}{4\pi} \right)^2 \mathcal{M}_{\text{fin}}^{(2)}, \quad (36)$$

where

$$\begin{aligned} \mathcal{M}_{\text{fin}}^{(0)} &= \mathcal{M}_{\text{ren}}^{(0)}, \\ \mathcal{M}_{\text{fin}}^{(1)} &= \mathcal{M}_{\text{ren}}^{(1)} - \mathbf{Z}^{(1)} \mathcal{M}_{\text{ren}}^{(0)}, \\ \mathcal{M}_{\text{fin}}^{(2)} &= \mathcal{M}_{\text{ren}}^{(2)} + ((\mathbf{Z}^{(1)})^2 - \mathbf{Z}^{(2)}) \mathcal{M}_{\text{ren}}^{(0)} - \mathbf{Z}^{(1)} \mathcal{M}_{\text{ren}}^{(1)}. \end{aligned} \quad (37)$$

All the IR divergences are canceled order by order on the right-hand side of the above equations, which serves as a strong check of our calculations.

The hard function for tW production in SCET is defined as $|\mathcal{M}_{\text{fin}}|^2$. The perturbative expansion of the hard function is

$$H = H^{(0)} + \frac{\alpha_s}{4\pi} H^{(1)} + \left(\frac{\alpha_s}{4\pi} \right)^2 H^{(2)}, \quad (38)$$

where

$$\begin{aligned} H^{(0)} &= |\mathcal{M}_{\text{fin}}^{(0)}|^2, \\ H^{(1)} &= \mathcal{M}_{\text{fin}}^{(1)} \mathcal{M}_{\text{fin}}^{(0)*} + \mathcal{M}_{\text{fin}}^{(0)} \mathcal{M}_{\text{fin}}^{(1)*}, \\ H^{(2)} &= \mathcal{M}_{\text{fin}}^{(2)} \mathcal{M}_{\text{fin}}^{(0)*} + \mathcal{M}_{\text{fin}}^{(0)} \mathcal{M}_{\text{fin}}^{(2)*} + |\mathcal{M}_{\text{fin}}^{(1)}|^2. \end{aligned} \quad (39)$$

We have obtained the result of $|\mathcal{M}_{\text{fin}}^{(1)}|^2$ with full color information in [19]. Similar to Eq. (5), the NNLO corrections to the hard function can be written as

$$\begin{aligned} H^{(2)} &= N_c^4 H_A + N_c^2 H_B + H_C + \frac{1}{N_c^2} H_D \\ &+ n_l \left(N_c^3 H_{El} + N_c H_{Fl} + \frac{1}{N_c} H_{Gl} \right) \\ &+ n_h \left(N_c^3 H_{Eh} + N_c H_{Fh} + \frac{1}{N_c} H_{Gh} \right). \end{aligned} \quad (40)$$

In this work, we provide the analytical result of the leading color contribution in Eq. (40), which is defined by

$$H_{\text{L.C.}}^{(2)} \equiv N_c^4 H_A, \quad (41)$$

as well as the one including the light fermion-loop contribution

$$H_{\text{L.C.}+n_l}^{(2)} \equiv N_c^4 H_A + n_l \left(N_c^3 H_{El} + N_c H_{Fl} + \frac{1}{N_c} H_{Gl} \right). \quad (42)$$

IV. NUMERICAL RESULTS

When we present the numerical results in this section, a factor $e^2 g_s^2 / \sin^2 \theta_W$ has been extracted out in the hard functions. The ratio between the mass of the W boson and that of the top quark is fixed to be $m_W^2 / m_t^2 = 3/14$ as in Ref. [19]. The renormalization scale μ is set to $m_t = 173$ GeV. The phase space is parametrized with the velocity β_t and polar angle θ of the final-state top quark in the center-of-mass frame of the initial-state partons, assuming that the incoming gluon moves in the z direction. The Mandelstam variables can be written as

$$\begin{aligned} s &= m_W^2 - m_t^2 + 2\Delta, & t &= m_t^2 - \Delta(1 + \beta_t \cos \theta), \\ u &= m_t^2 - \Delta(1 - \beta_t \cos \theta) \end{aligned} \quad (43)$$

with $\Delta = (m_t^2 + m_t \sqrt{m_W^2 + \beta_t^2 (m_t^2 - m_W^2)}) / (1 - \beta_t^2)$. The phase space constraints are $0 \leq \beta_t < 1$ and $-1 \leq \cos \theta \leq 1$. We generate a grid of 3360 points in these regions. The numerical evaluation of the squared amplitudes at each phase space point takes about a few minutes on a single core, and the relative precision is around 10^{-10} . When performing phase space integration, one needs the values of the squared amplitudes at points in the intermediate region.

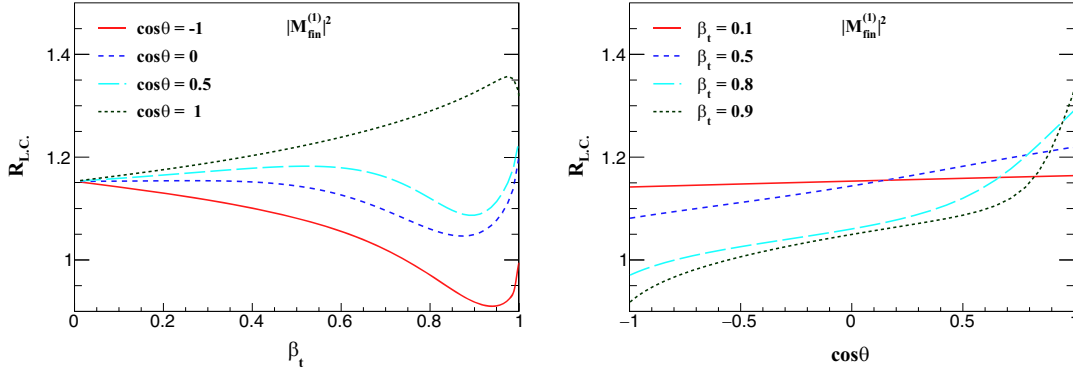


FIG. 6. Ratio of the leading color contribution of $|\mathcal{M}_{\text{fin}}^{(1)}|^2$ to the one with full color dependence. The left plot shows the β_t distribution with $\cos\theta$ fixed at -1 (red), 0 (blue), 0.5 (cyan), and 1 (dark green). The right plot presents the ratio over $\cos\theta$ with β_t fixed at 0.1 (red), 0.5 (blue), 0.8 (cyan), and 0.9 (dark green).

These can be easily obtained using an interpolation method. We check that the derived values agree with the ones from direct computation within an accuracy of at worst 10^{-3} , which is sufficient for a phenomenological study. The numerical results of the two-loop amplitudes on this grid as well as the analytical results are available from the authors upon request.

We present the leading color result of the hard function in this paper and expect that this represents the dominant contribution, as we argued in Sec. II A. To illustrate this in practice, we examine the one-loop squared matrix element

$|\mathcal{M}_{\text{fin}}^{(1)}|^2$, which is known with full color dependence [19]. It is convenient to define the ratio $R_{\text{L.C.}} = |\mathcal{M}_{\text{fin}}^{(1)\text{L.C.}}|^2 / |\mathcal{M}_{\text{fin}}^{(1)}|^2$, which is a function of β_t and $\cos\theta$. Then, $1 - R_{\text{L.C.}}$ estimates the effect of $1/N_c^2$ suppressed, dubbed subleading color, contributions. The numerical result of $R_{\text{L.C.}}$ is presented in Fig. 6. In the small β_t region ($\beta_t \leq 0.2$), $R_{\text{L.C.}}$ is around 1.15 , insensitive to the variation of $\cos\theta$. As β_t increases, the dependence of $R_{\text{L.C.}}$ on $\cos\theta$ becomes stronger, and $R_{\text{L.C.}}$ can grow to 1.36 or decrease to 0.91 at most. However, $|1 - R_{\text{L.C.}}|$ is less than 20% except for the

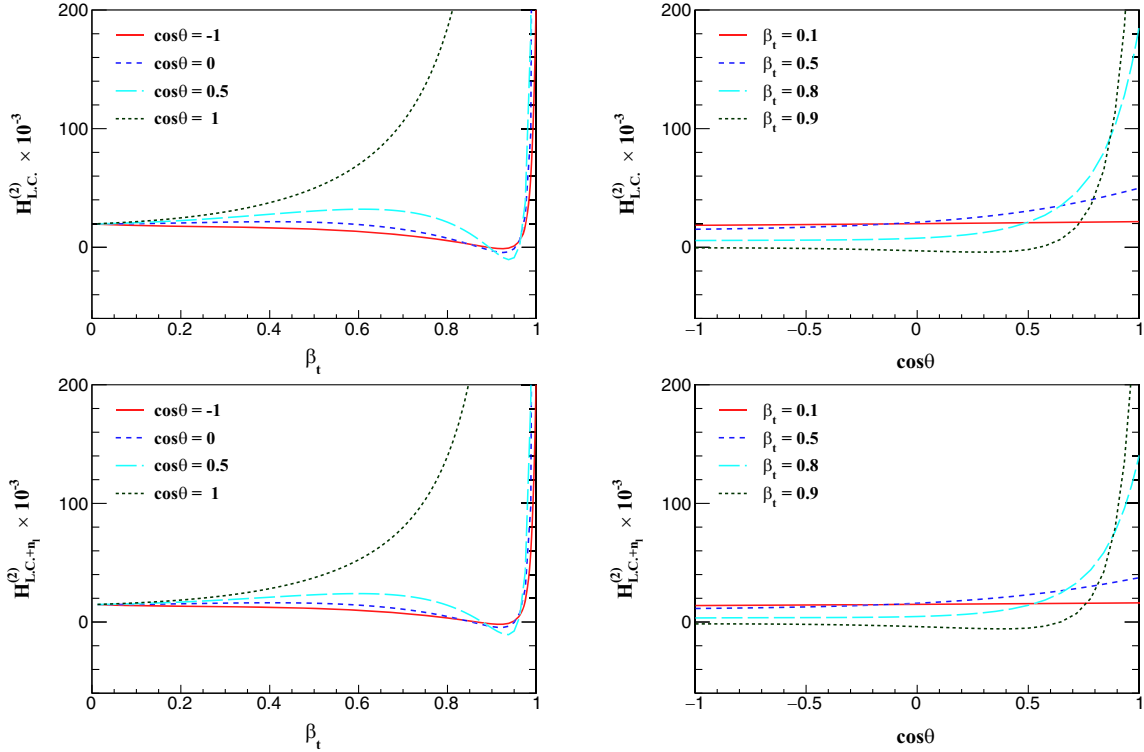
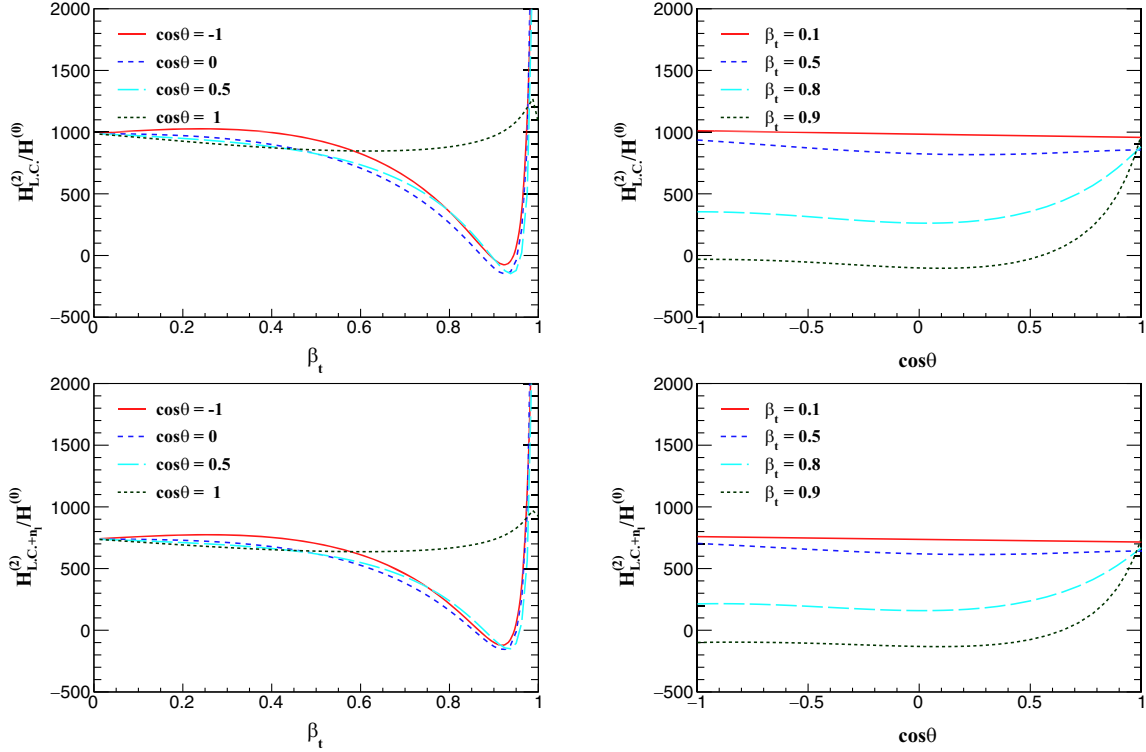


FIG. 7. Leading color (top panel) and the sum of leading color and light fermion-loop contributions (bottom panel) to the NNLO hard functions.

FIG. 8. Same as Fig. 7 but normalized by $H^{(0)}$.

region with $\beta_t \geq 0.8$ and $\cos \theta \geq 0.8$, which indicates that the leading color result is the dominant contribution, as expected.

Then, we turn to the leading color NNLO hard function. As shown in Fig. 7, it changes very slowly in the region with $\beta_t \leq 0.7$ and $\cos \theta \leq 0.6$. For small β_t , this flat region extends to almost the whole $\cos \theta$ range. But the leading color hard function quickly becomes divergent for large β_t and general $\cos \theta$. This reflects the fact that the amplitude develops new singularities in the limit $m_t \rightarrow 0$. One can also observe the strongest divergence in the case of $\cos \theta = 1$. This behavior is due to the tree-level propagator that contains $1/(1 - \beta_t \cos \theta)$. This kind of divergence should cancel in the ratio $H^{(2)}/H^{(0)}$, as displayed in Fig. 8. However, the divergences arising from higher-order corrections, which are manifested in the logarithmic terms $\ln(1 - \beta_t^2)$, $\ln(1 - \beta_t \cos \theta)$, and $\ln(1 + \beta_t \cos \theta)$, survive in the ratio. Though they are numerically large, the hadronic cross section still drops dramatically as $\beta_t \rightarrow 1$ due to the overwhelming suppression of the parton distribution function [19]. Therefore, we do not need to worry about the divergent behavior in Fig. 8.

The light fermion-loop diagrams may also be important due to the large value of n_l . In Figs. 7 and 8, we also show the numerical result of the hard function defined in Eq. (42), which includes such additional contributions. We find that the light fermion-loop diagrams provide negative contributions and decrease the leading color result by about 30% in most of the phase space. To be more

specific and realistic, we perform the convolution with parton distribution functions⁶ and integrate over all phase space, observing that the leading color and n_l dependent parts of the NNLO hard function contribute about 5.4% and -1.4% , respectively, corrections to the LO cross section at the 13 TeV LHC.

V. CONCLUSION

We have computed the two-loop virtual corrections to tW production at hadron colliders, focusing on the leading color and light fermion-loop contributions. Using the method of differential equations, the results are obtained in terms of multiple polylogarithms. After renormalization, we find that the IR divergences exhibit a structure that is fully determined by the anomalous dimensions, which are known in the literature. The finite part of the two-loop amplitude contributes to the hard function, which is an essential ingredient for a NNLO Monte Carlo calculation. Numerical evaluation of the one-loop squared amplitude confirms that the leading color result gives the dominant contribution. The leading color NNLO hard function shows very weak kinematic dependence in the region where the velocity β_t of the top quark is small. But it increases dramatically as β_t approaches 1. This behavior is caused by

⁶We use CT14NLO [53] with LHAPDF6 [54] in practical calculation, and the factorization and renormalization scales are set at m_t .

two kinds of singularities. The first kind of singularity, which arises due to the on-shell propagator, disappears after normalization by the LO hard function, while the second still exists as logarithmic terms. However, they do not have a large impact on the hadronic cross section due to the suppression of the parton distribution function in the region of $\beta_t \rightarrow 1$. The light fermion-loop contribution is negative, amounting to 30% of the leading color result. The sum of the leading color and light fermion-loop contributions to the NNLO hard function increases the LO cross section by about 4% at the 13 TeV LHC.

Combined with the NNLO N -jettiness soft function [55,56] and beam functions [57,58], it is now promising to calculate the dominant NNLO QCD correction to the cross section of tW production using the N -jettiness subtraction method [59–61].

The analytical results of full color two-loop amplitudes are difficult to obtain due to multiple elliptic curves, which some master integrals beyond leading color may depend on. However, it is feasible to calculate them numerically thanks to the recent developments, such as the AMFlow [62] and SeaSyde [63] packages or the method proposed in [64]. We leave this to future work.

ACKNOWLEDGMENTS

This work was supported in part by the National Science Foundation of China under Grants No. 12005117, No. 12075251, No. 12147154, No. 12275156, and No. 12175048. The work of L. D. and J. W. was also supported by the Taishan Scholar Foundation of Shandong province (tsqn201909011).

-
- [1] M. Aaboud *et al.* (ATLAS Collaboration), Measurement of the cross-section for producing a W boson in association with a single top quark in pp collisions at $\sqrt{s} = 13$ TeV with ATLAS, *J. High Energy Phys.* **01** (2018) 063.
 - [2] M. Aaboud *et al.* (ATLAS Collaboration), Measurement of differential cross-sections of a single top quark produced in association with a W boson at $\sqrt{s} = 13$ TeV with ATLAS, *Eur. Phys. J. C* **78**, 186 (2018).
 - [3] A. M. Sirunyan *et al.* (CMS Collaboration), Measurement of the production cross section for single top quarks in association with W bosons in proton-proton collisions at $\sqrt{s} = 13$ TeV, *J. High Energy Phys.* **10** (2018) 117.
 - [4] A. Tumasyan *et al.* (CMS Collaboration), Observation of tW production in the single-lepton channel in pp collisions at $\sqrt{s} = 13$ TeV, *J. High Energy Phys.* **11** (2021) 111.
 - [5] W. T. Giele, S. Keller, and E. Laenen, QCD corrections to W boson plus heavy quark production at the Tevatron, *Phys. Lett. B* **372**, 141 (1996).
 - [6] S. Zhu, Next-to-leading order QCD corrections to $bg \rightarrow tW^-$ at CERN large hadron collider, *Phys. Lett. B* **524**, 283 (2002).
 - [7] J. M. Campbell and F. Tramontano, Next-to-leading order corrections to Wt production and decay, *Nucl. Phys.* **B726**, 109 (2005).
 - [8] Q.-H. Cao, Demonstration of one cutoff phase space slicing method: Next-to-leading order QCD corrections to the tW associated production in hadron collision, [arXiv:0801.1539](https://arxiv.org/abs/0801.1539).
 - [9] P. Kant, O. M. Kind, T. Kintscher, T. Lohse, T. Martini, S. Mölbitz, P. Rieck, and P. Uwer, HatHor for single top-quark production: Updated predictions and uncertainty estimates for single top-quark production in hadronic collisions, *Comput. Phys. Commun.* **191**, 74 (2015).
 - [10] N. Kidonakis, Single top production at the Tevatron: Threshold resummation and finite-order soft gluon corrections, *Phys. Rev. D* **74**, 114012 (2006).
 - [11] N. Kidonakis, Two-loop soft anomalous dimensions for single top quark associated production with a W^- or H^- , *Phys. Rev. D* **82**, 054018 (2010).
 - [12] N. Kidonakis, Soft-gluon corrections for tW production at N^3 LO, *Phys. Rev. D* **96**, 034014 (2017).
 - [13] N. Kidonakis and N. Yamanaka, Higher-order corrections for tW production at high-energy hadron colliders, *J. High Energy Phys.* **05** (2021) 278.
 - [14] C. S. Li, H. T. Li, D. Y. Shao, and J. Wang, Momentum-space threshold resummation in tW production at the LHC, *J. High Energy Phys.* **06** (2019) 125.
 - [15] S. Frixione, E. Laenen, P. Motylinski, B. R. Webber, and C. D. White, Single-top hadroproduction in association with a W boson, *J. High Energy Phys.* **07** (2008) 029.
 - [16] E. Re, Single-top Wt -channel production matched with parton showers using the POWHEG method, *Eur. Phys. J. C* **71**, 1547 (2011).
 - [17] T. Ježo, J. M. Lindert, P. Nason, C. Oleari, and S. Pozzorini, An NLO + PS generator for $t\bar{t}$ and Wt production and decay including non-resonant and interference effects, *Eur. Phys. J. C* **76**, 691 (2016).
 - [18] F. Demartin, B. Maier, F. Maltoni, K. Mawatari, and M. Zaro, tWH associated production at the LHC, *Eur. Phys. J. C* **77**, 34 (2017).
 - [19] L.-B. Chen, L. Dong, H. T. Li, Z. Li, J. Wang, and Y. Wang, One-loop squared amplitudes for hadronic tW production at next-to-next-to-leading order in QCD, *J. High Energy Phys.* **08** (2022) 211.
 - [20] Z. Bern and D. A. Kosower, Color decomposition of one loop amplitudes in gauge theories, *Nucl. Phys.* **B362**, 389 (1991).
 - [21] T. Hahn, Generating Feynman diagrams and amplitudes with FeynArts 3, *Comput. Phys. Commun.* **140**, 418 (2001).
 - [22] V. Shtabovenko, R. Mertig, and F. Orellana, FeynCalc 9.3: New features and improvements, *Comput. Phys. Commun.* **256**, 107478 (2020).

- [23] J. G. Korner, D. Kreimer, and K. Schilcher, A practicable $\gamma(5)$ scheme in dimensional regularization, *Z. Phys. C* **54**, 503 (1992).
- [24] A. V. Smirnov and F. S. Chuharev, FIRE6: Feynman Integral REduction with Modular Arithmetic, *Comput. Phys. Commun.* **247**, 106877 (2020).
- [25] A. V. Kotikov, Differential equations method: New technique for massive Feynman diagrams calculation, *Phys. Lett. B* **254**, 158 (1991).
- [26] A. V. Kotikov, Differential equation method: The calculation of N point Feynman diagrams, *Phys. Lett. B* **267**, 123 (1991).
- [27] J. M. Henn, Multiloop Integrals in Dimensional Regularization Made Simple, *Phys. Rev. Lett.* **110**, 251601 (2013).
- [28] K.-T. Chen, Iterated path integrals, *Bull. Am. Math. Soc.* **83**, 831 (1977).
- [29] A. B. Goncharov, Multiple polylogarithms, cyclotomy and modular complexes, *Math. Res. Lett.* **5**, 497 (1998).
- [30] C. Duhr and F. Dulat, PolyLogTools—Polylogs for the masses, *J. High Energy Phys.* **08** (2019) 135.
- [31] J. Vollinga and S. Weinzierl, Numerical evaluation of multiple polylogarithms, *Comput. Phys. Commun.* **167**, 177 (2005).
- [32] C. W. Bauer, A. Frink, and R. Kreckel, Introduction to the GiNaC framework for symbolic computation within the C++ programming language, *J. Symb. Comput.* **33**, 1 (2002).
- [33] L.-B. Chen and J. Wang, Analytic two-loop master integrals for tW production at hadron colliders: I *, *Chin. Phys. C* **45**, 123106 (2021).
- [34] M.-M. Long, R.-Y. Zhang, W.-G. Ma, Y. Jiang, L. Han, Z. Li *et al.*, Two-loop master integrals for the single top production associated with W boson, [arXiv:2111.14172](https://arxiv.org/abs/2111.14172).
- [35] J. Wang and Y. Wang, Analytic two-loop master integrals for tW production at hadron colliders: II, [arXiv:2211.13713](https://arxiv.org/abs/2211.13713).
- [36] L.-B. Chen, Y. Liang, and C.-F. Qiao, Two-Loop integrals for CP -even heavy quarkonium production and decays, *J. High Energy Phys.* **06** (2017) 025.
- [37] D. J. Broadhurst, N. Gray, and K. Schilcher, Gauge invariant on-shell $Z(2)$ in QED, QCD and the effective field theory of a static quark, *Z. Phys. C* **52**, 111 (1991).
- [38] K. Melnikov and T. van Ritbergen, The three loop on-shell renormalization of QCD and QED, *Nucl. Phys.* **B591**, 515 (2000).
- [39] M. Czakon, A. Mitov, and S. Moch, Heavy-quark production in gluon fusion at two loops in QCD, *Nucl. Phys.* **B798**, 210 (2008).
- [40] M. Czakon, A. Mitov, and S. Moch, Heavy-quark production in massless quark scattering at two loops in QCD, *Phys. Lett. B* **651**, 147 (2007).
- [41] S. Catani, The singular behavior of QCD amplitudes at two loop order, *Phys. Lett. B* **427**, 161 (1998).
- [42] T. Becher and M. Neubert, Infrared Singularities of Scattering Amplitudes in Perturbative QCD, *Phys. Rev. Lett.* **102**, 162001 (2009).
- [43] E. Gardi and L. Magnea, Factorization constraints for soft anomalous dimensions in QCD scattering amplitudes, *J. High Energy Phys.* **03** (2009) 079.
- [44] T. Becher and M. Neubert, On the structure of infrared singularities of gauge-theory amplitudes, *J. High Energy Phys.* **06** (2009) 081.
- [45] T. Becher and M. Neubert, Infrared singularities of QCD amplitudes with massive partons, *Phys. Rev. D* **79**, 125004 (2009).
- [46] A. Ferroglia, M. Neubert, B. D. Pecjak, and L. L. Yang, Two-Loop Divergences of Scattering Amplitudes with Massive Partons, *Phys. Rev. Lett.* **103**, 201601 (2009).
- [47] A. Mitov, G. F. Sterman, and I. Sung, Computation of the soft anomalous dimension matrix in coordinate space, *Phys. Rev. D* **82**, 034020 (2010).
- [48] N. Kidonakis, Soft anomalous dimensions for single-top production at three loops, *Phys. Rev. D* **99**, 074024 (2019).
- [49] Z. L. Liu and N. Schalch, Infrared singularities of multi-leg QCD amplitudes with a massive parton at three loops, [arXiv:2207.02864](https://arxiv.org/abs/2207.02864).
- [50] S. Catani and M. H. Seymour, The dipole formalism for the calculation of QCD jet cross-sections at next-to-leading order, *Phys. Lett. B* **378**, 287 (1996).
- [51] H. T. Li, C. S. Li, D. Y. Shao, L. L. Yang, and H. X. Zhu, Top quark pair production at small transverse momentum in hadronic collisions, *Phys. Rev. D* **88**, 074004 (2013).
- [52] M. Steinhauser, Results and techniques of multiloop calculations, *Phys. Rep.* **364**, 247 (2002).
- [53] S. Dulat, T.-J. Hou, J. Gao, M. Guzzi, J. Huston, P. Nadolsky, J. Pumplin, C. Schmidt, D. Stump, and C.-P. Yuan, New parton distribution functions from a global analysis of quantum chromodynamics, *Phys. Rev. D* **93**, 033006 (2016).
- [54] A. Buckley, J. Ferrando, S. Lloyd, K. Nordström, B. Page, M. Rüfenacht, M. Schönherr, and G. Watt, LHAPDF6: Parton density access in the LHC precision era, *Eur. Phys. J. C* **75**, 132 (2015).
- [55] H. T. Li and J. Wang, Next-to-next-to-leading order N -jettiness soft function for one massive colored particle production at hadron colliders, *J. High Energy Phys.* **02** (2017) 002.
- [56] H. T. Li and J. Wang, Next-to-next-to-leading order N -jettiness soft function for tW production, *Phys. Lett. B* **784**, 397 (2018).
- [57] J. R. Gaunt, M. Stahlhofen, and F. J. Tackmann, The quark beam function at two loops, *J. High Energy Phys.* **04** (2014) 113.
- [58] J. Gaunt, M. Stahlhofen, and F. J. Tackmann, The gluon beam function at two loops, *J. High Energy Phys.* **08** (2014) 020.
- [59] J. Gao, C. S. Li, and H. X. Zhu, Top Quark Decay at Next-to-Next-to-Leading Order in QCD, *Phys. Rev. Lett.* **110**, 042001 (2013).
- [60] R. Boughezal, C. Focke, X. Liu, and F. Petriello, W -Boson Production in Association with a Jet at Next-to-Next-to-Leading Order in Perturbative QCD, *Phys. Rev. Lett.* **115**, 062002 (2015).
- [61] J. Gaunt, M. Stahlhofen, F. J. Tackmann, and J. R. Walsh, N -jettiness subtractions for NNLO QCD calculations, *J. High Energy Phys.* **09** (2015) 058.

- [62] X. Liu and Y.-Q. Ma, AMFlow: A Mathematica package for Feynman integrals computation via auxiliary mass flow, *Comput. Phys. Commun.* **283**, 108565 (2023).
- [63] T. Armadillo, R. Bonciani, S. Devoto, N. Rana, and A. Vicini, Evaluation of Feynman integrals with arbitrary complex masses via series expansions, *Comput. Phys. Commun.* **282**, 108545 (2023).
- [64] M. Hidding and J. Usovitsch, Feynman parameter integration through differential equations, [arXiv:2206.14790](https://arxiv.org/abs/2206.14790).